International Journal of Fatigue 61 (2014) 10–20

Contents lists available at ScienceDirect

International Journal of Fatigue

journal homepage: www.elsevier.com/locate/ijfatigue

Investigation of thermal effects on fatigue crack closure using multiscale digital image correlation experiments

Mallory C. Casperson [a,*], Jay D. Carroll [b,1], John Lambros [a], Huseyin Sehitoglu [b], Robert H. Dodds jr. [c]

[a] Department of Aerospace Engineering, University of Illinois at Urbana-Champaign, 104 S. Wright Street, Urbana, IL 61801, USA
[b] Department of Mechanical Science and Engineering, University of Illinois at Urbana-Champaign, 1206 W. Green Street, Urbana, IL 61801, USA
[c] Department of Civil and Environmental Engineering, University of Illinois at Urbana-Champaign, 205 N. Mathews Ave., Urbana, IL 61801, USA

ARTICLE INFO

Article history:
Received 13 April 2013
Received in revised form 22 November 2013
Accepted 27 November 2013
Available online 6 December 2013

Keywords:
Fatigue crack closure
Crack growth rate
High temperature
Thermal overload
Blunting

ABSTRACT

Hastelloy X, a nickel-based superalloy, has been extensively used for high temperature applications. In this work, Hastelloy X notched samples were used to investigate fatigue crack growth and crack closure at elevated temperatures. Isothermal, thermal jump, and thermal overload experiments at varying temperatures (up to 650 °C), were performed. Macroscale (2 μm/pixel) digital image correlation was performed on images taken at various stages of crack growth and microscale (0.4 μm/pixel) digital image correlation was used on images obtained directly behind the crack tip to quantify the local effects of crack closure. Experiments focused on the effects of isothermal conditions and thermal overloads on measured crack closure levels. Each isothermal experiment showed steady state crack closure levels of 0.30 while thermal jumps and thermal overloads created significant decreases (or, in some cases, complete elimination) in closure levels immediately following the temperature change. Similar to the case of mechanical overloads, as crack growth was continued beyond the plastic zone enlargement created by the thermal spike, closure levels were reestablished near the original steady state values. Competing mechanisms, including crack tip blunting, crack bifurcation, change in temperature, yield stress, elastic modulus, and plastic zone size, thought to be responsible for the changes in closure levels following the thermal jumps and during the thermal overload, were investigated.

1. Introduction

Over the past 100 years, extensive research has taken place in order to create a damage tolerant design approach incorporating possible fatigue damage of a structural component. The stress intensity factor has been employed as a key variable in predicting fatigue life. Early research into this area performed by Paris and Erdogan [1] and McEvily and Boettner [2] related fatigue crack growth rate, da/dN, to the stress intensity factor range, ΔK, through the well-known Paris relationship.

As a fatigue crack grows in a ductile material, it leaves behind a plastic wake. This plastic wake produces compressive forces that shield the crack from external loading. As a result, the crack does not fully open until a specific opening load is reached. This phenomenon, which causes the crack to "unzip" when loaded, is known as crack closure. In 1970, Elber discovered a relationship between crack growth rates and crack closure [3,4]. The conventional Paris relationship was thus modified by Elber to incorporate only the portion of the loading range, or the effective stress intensity factor range, experienced by the opened crack [3,4] as,

$$\frac{da}{dN} = C(\Delta K_{eff})^m, \quad \Delta K_{eff} = K_{max} - K_{open}, \tag{1}$$

where da/dN is the crack growth rate for the effective stress intensity factor range, ΔK_{eff}. Various types of crack closure have been identified, including plasticity-, oxide-, roughness-, viscous fluid-, and phase transformation-induced crack closure [5].

Elber showed that a compliance change accompanied opening of the crack and that, by using a displacement gauge 2 mm behind the crack tip to measure the relative opening of the crack, the load level corresponding to the compliance change could be measured. Sehitoglu [6] found that crack opening load levels are typically higher than crack closing load levels and reach saturated levels with increasing crack length. Davidson [7] confirmed earlier statements by Horng and Fine [8] and Veccio et al. [9] that closure levels are different in center-notch specimens than for single-edge notch specimens. Carroll et al. [10] used macroscale and microscale methods to study crack closure of Ti at room temperature.

In this work, full-field methods developed by Carroll et al. in Ti specimens were employed. These methods included two different macroscale techniques for measuring crack closure through

* Corresponding author.
E-mail address: mallory.casperson@gmail.com (M.C. Casperson).
[1] Current address: Sandia National Laboratories, PO Box 5800, Albuquerque, NM 87185-0889, USA

0142-1123/$ - see front matter © 2013 Elsevier Ltd. All rights reserved.
http://dx.doi.org/10.1016/j.ijfatigue.2013.11.020

full-field measurements of stress intensity factors using digital image correlation (DIC). One method compared the measured stress intensity factor to the theoretical stress intensity factor in the absence of crack closure. The second method determined the crack opening level by a slope change in the stress intensity factor vs. load curve. These techniques, along with the local displacement gauge techniques of Riddell et al. [11] and Sutton et al. [12] were used to provide multiscale measurements of fatigue crack opening and closure loads.

Engineering components are often subjected to mechanically and thermally varying environments. Mechanical overloads have been extensively studied [13–21] but less is known about the impact of thermal overloads on fatigue crack growth even though high temperatures significantly affect material properties [22]. Some work has been done with crack closure at high temperature isothermal conditions. Babu et al. [23] studied stainless steel 316(N) weld metal and identified that roughness-induced crack closure was present at 300 K, while oxide-induced crack closure was present at 823 K. Kokini [24] succeeded in using a displacement method as well as a modified crack closure integral method to calculate stress intensity factors using finite element analysis for a cracked strip undergoing a thermal shock. Similarly, Giannopoulos and Anifantis [25] used finite element analysis to study two-dimensional crack closure under variable heating.

The present investigation is concerned with the effects of elevated temperature and thermal history on fatigue crack closure including isothermal, thermal jump (where one steady state thermal condition is elevated to another during fatigue loading), and thermal overload (where a single cycle temperature spike occurs during fatigue loading) conditions. Digital image correlation techniques were employed to quantify the levels of crack closure a specimen experienced as a function of thermal history. Crack propagation rates following a thermal overload, as well as crack tip blunting, crack bifurcation, and plastic zone size were considered. Section 2 explores the experimental methods and procedures used to quantify deformation at high temperature. In Section 3.1, the crack closure results are shown for the isothermal experiments at two different measurement length scales (micro- and macro-scale). The results from the thermal jump and thermal overload experiments are finally discussed in Sections 3.2 and 3.3.

2. Experimental methods

2.1. Material and specimen preparation

The single edge notch tension specimens used in this investigation were 75 mm by 7.0 mm by 1.3 mm pieces cut from a plate of Hastelloy X using wire electrical discharge machining (EDM). Hastelloy X is a nickel-based superalloy with an average grain size of 50 μm, and profuse annealing twins throughout the material [26]. Temperature dependent material properties for Hastelloy X, as provided by Haynes International are plotted in Fig. 1. Evolution of uniaxial stress–strain curves of Hastelloy X at various temperatures can be seen in [27]. Varying batches of Hastelloy X have been found to exhibit slightly different stress–strain behavior as a function of temperature due to inherent differences in the material.

Along one edge of the rectangular sample, a 1 mm long notch was cut using a 0.15 mm EDM wire. The specimen was then polished using 320, 600, and 800 grit polishing paper, successively. A speckle pattern was applied to the polished surface for DIC. The speckle patterns were made of either high temperature paint or 1–5 μm silicon particles adhered using a compressed air application technique [28,29]. The high temperature painting method of applying a speckle pattern is similar to the procedure developed by Efstathiou et al. for studying intermartensitic transformations in single-crystal NiFeGa [30] and was used in the earliest experiments. The silicon particle speckle pattern was used for the majority of the experiments described here as this method more easily facilitates identification of the crack tip during testing.

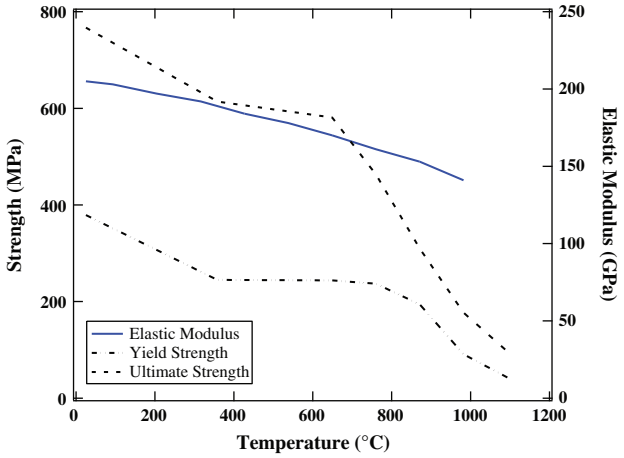

Fig. 1. Temperature dependence of elastic modulus and ultimate and yield strengths of Hastelloy X as provided by the manufacturer, Haynes International [31].

For these high temperature experiments, in addition to the speckle pattern deposited on the front surface of the sample, the back surface was painted with a high temperature, flat black paint to increase sample emissivity. This allowed the use of a Raytek infrared thermometer to monitor the specimen's temperature. In earlier efforts it was found that this infrared thermometer accurately captures the temperature of the specimen within ±10 °C.

2.2. Experimental procedure

In order to initiate and grow a crack from the notch tip, the specimen was fatigue loaded in axial tension at a frequency of 2 Hz using an Instron 8802 servohydraulic load frame in what will henceforth be referred to as "precracking." During the fatigue precracking, the theoretical mode I stress intensity factor, K_I, calculated for the single edge notch geometry used in this investigation, was maintained at 19 ± 2 MPa $\sqrt{m}$ by load shedding. K_I can be calculated by,

$$K_I = F\sigma\sqrt{\pi a} \tag{2}$$

where F is the dimensionless function given by Eq. (3), σ is the applied stress, and a is the total length of the crack (notch plus fatigue crack). In the expression for F, given by

$$F = 0.265(1-\alpha)^4 + \frac{0.857 + 0.265\alpha}{(1-\alpha)^{\frac{3}{2}}}, \tag{3}$$

and α is the crack length divided by the specimen width [32].

Images were taken during the precracking cycles at a rate of 8 images per cycle, using a Navitar 12× zoom lens with 2× adapter tube, and an IMI-1200FT digital camera with a 1600 × 1200 resolution, and then inspected in order to most accurately determine the crack length. Lighting was provided by fiber optic gooseneck lights as well as a fiber optic ring light. The load frame and the camera were synchronized by a LabView program. Fig. 2(a) shows the entire experimental set up used for all experiments in this work while Fig. 2(b) shows the red box from Figure (a) at a higher magnification. During loading, the load ratio R, the ratio of minimum load to maximum load, was maintained at 0.05 as to facilitate the presence of crack closure. With the crack grown to a total length (including the notch) of between 2.2 mm and 2.4 mm from

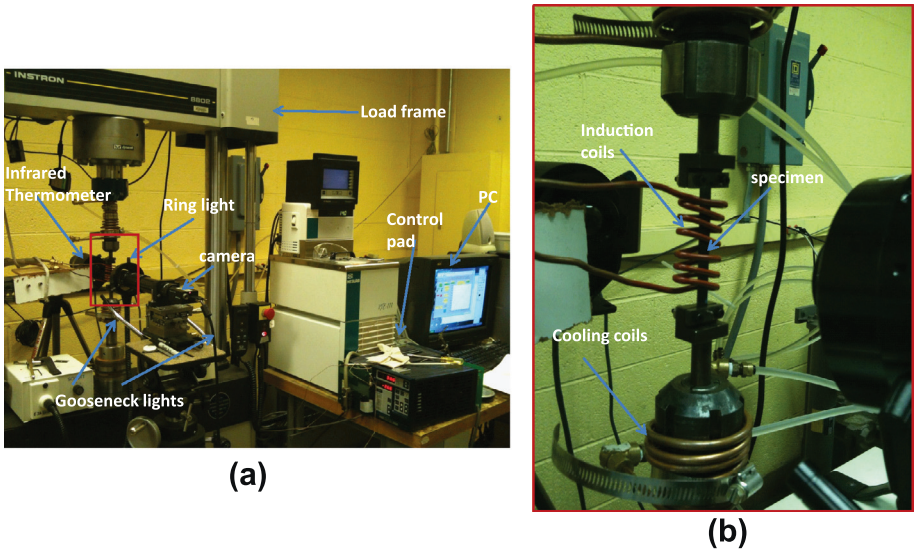

Fig. 2. Experimental set up for all experiments. Each component of the set up is labeled, including a red boxed area that is shown at a higher magnification in (b). (For interpretation of the references to color in this figure legend, the reader is referred to the web version of this article.)

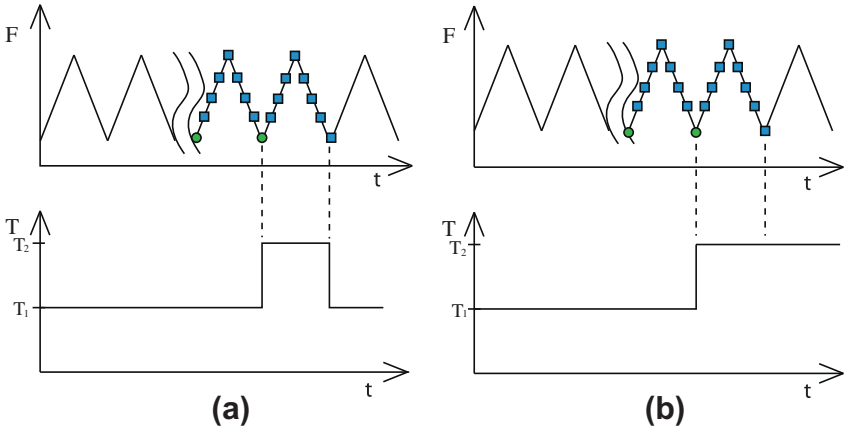

Fig. 3. (a) Thermal overload thermal (bottom) and mechanical (top) loading profiles. (b) Thermal jump thermal (bottom) and mechanical (top) loading profiles.

the edge of the specimen, loading was halted and the specimen was subjected to several cycles, run at the same load amplitude as the final cycles of fatigue precracking but at a lower frequency of 0.125 Hz. During these lower frequency cycles, referred to as "measurement cycles," images were taken at 15 frames per second, totaling 120 images per cycle.

The effects of temperature on fatigue crack closure were then investigated in terms of (i) isothermal, (ii) thermal jump, and (iii) thermal overload fatigue crack growth experiments. The distinction between each type of experiment occurred only after fatigue precracking of the specimen. Heating was performed using a Lepel Induction heater to generate currents in the conductive Hastelloy X sample. Copper tubing, 3.175 mm in diameter, bent into an elliptically shaped coil, surrounded the specimen. Heating for each type of experiment was performed with the specimen mounted in the load frame and specimens were not removed before testing was completed.

Adapting the methods of Carroll et al. for room temperature crack closure [10], isothermal experiments were run at room temperature (denoted as RT), 300 °C, and 550 °C. The specimen was heated to the desired temperature (T_1), fatigue precracking to the desired crack length was performed under isothermal, T_1, conditions, and several measurement cycles were completed in order to quantify crack closure. The thermal (bottom) and mechanical (top) histories for the thermal overload and thermal jump experiments are shown in Fig. 3(a) and (b), respectively. As seen in the figure, the mechanical loading history is the same for both the thermal overload (Fig. 3(a)) and the thermal jump (Fig. 3(b)) experiments. Fatigue precracking occurred at constant ΔK (shown before the two, interrupted lines indicating that many thousands of cycles were performed) until the desired crack length was reached. Then a series of slower measurement cycles were performed to quantify crack closure during a complete loading cycle. DIC was performed during the measurement cycles, thus the green dot signifies the reference image at minimum load and the blue squares represent the deformed images taken during the loading cycle.

The bottom schematics in Fig. 3 show the thermal loading histories. The thermal jump experiment is an abbreviated version of the thermal overload experiment. In the thermal jump experiment (Fig. 3(b)), T_1 was maintained constant during the fatigue precracking as well as an initial round of measurement cycles (as shown by comparing the thermal profile directly with the mechanical one above it). The temperature was then raised to T_2, and another series of measurement cycles were performed. The thermal history used in the thermal overload experiment began exactly in the same way as the thermal jump experiment. Then, following the

measurement cycles at T_2, the temperature was lowered back to T_1 and fatigue cracking of the specimen was resumed. Measurement cycles were then performed periodically as the crack advanced, at numerous crack lengths. In this way, crack closure measurements as a function of crack length and thermal history were made.

2.3. Multiscale high-temperature digital image correlation

DIC analysis of the images taken during the measurement cycles was done using a commercially available digital image correlation software, Vic2D (from Correlated Solutions Inc.). DIC provides a measurement of the in-plane displacement and displacement gradient components of a flat, two-dimensional (2D) surface. The details of DIC are well known in the literature [11,33,34] and are not discussed here except to remind the reader that square subsets are defined in a reference image (here, the minimum load image is used as the reference) and are located in each subsequent, deformed image in order to calculate the deformation incurred during loading. The subset size provides an estimate of the spatial resolution of the measurement made.

In the past, DIC studies have been undertaken at high temperatures by a number of researchers. Lyons et al. [35] were among the first to use DIC to obtain full-field deformation measurements at temperatures up to 650 °C. They validated that the DIC method was able to accurately measure mechanically and thermally induced strains at high temperatures. Grant et al. [36] used a similar experimental method to test this same hypothesis, though without the use of a physical speckle pattern applied to the specimen surface and using blue illumination and bandpass filter. They were able to measure the Young's modulus and the coefficient of thermal expansion up to temperatures of 1000 °C. Pan et al. [37] applied these same methods to measure deformation for a temperature range of room temperature to 1200 °C. It is important to note however, that none of these studies investigated fatigue at high temperatures with DIC measurement techniques.

High temperature DIC experiments pose additional and unique challenges to those typically associated with room temperature DIC experiments. The speckle pattern must adhere to the specimen when heated. In order for correlations between the reference subsets and the deformed subsets to be successful, the light intensity must remain relatively constant between the two configurations. This becomes more complicated at higher temperatures since most metallic surfaces oxidize when heated. Therefore, prior to performing a high temperature experiment, the specimen was kept at zero load while mounted in the load frame, and then preoxidized to the T_2 temperature until a steady state of oxidation was reached on the specimen's surface. The specimen was then cooled to the T_1 temperature and precracking was started. In the case of an isothermal experiment, the specimen was preoxidized to the T_1 temperature until a steady state of oxidation was reached, prior to testing.

Using images obtained directly behind the crack tip during the measurement cycles, DIC was used to quantify the effects of crack closure. Carroll et al. [10] used DIC to study the effects of crack closure on Titanium at room temperature and Pataky et al. [38] used DIC to study crack closure in Haynes 230 at high temperatures. Using similar techniques in the current investigation, macroscale, full-field DIC measurements (using images taken at 2× magnification, 2 μm/pixel) were used to calculate global closure levels of Hastelloy X, while microscale DIC measurements (images taken at 10× magnification, 0.4 μm/pixel) were used to investigate local crack closure levels in the specimen as a function of distance from the tip of the fatigue crack.

Fig. 4 shows the regions of interest (ROI) used in the DIC analysis. The large red area is the ROI analyzed in the 2× magnification experiments while the smaller, yellow box is the ROI analyzed in the 10× magnification experiments. The tip of the initial notch is seen on the left of the zoomed in view as well as on the specimen schematic. The blue box represents the subset size, 41 × 41 pixels (82 × 82 μm), used during the correlations of the 2× magnification images. Within the yellow box, the crack tip is labeled with a red dot and the digital extensometers are placed along the crack line. During these measurement cycles, the crack is assumed to incur no further growth Although the points very near the crack tip were not excluded, this is expected to have a small effect on measured K values.

The microscale images (10×) were analyzed using a digital extensometer method where virtual displacement gauges, pairs of individual DIC subsets, were placed on either flank of the crack at various locations behind the crack tip as shown in Fig. 5. The yellow boxes in Fig. 5 are these subsets serving as virtual extensometers. With subset sizes of 71 × 71 (28 × 28 μm) to 101 × 101 pixels (40 × 40 μm) (depending on the exact resolution of the images), these extensometers measured crack opening and crack closing, at various locations behind the crack tip, along the length of the crack.

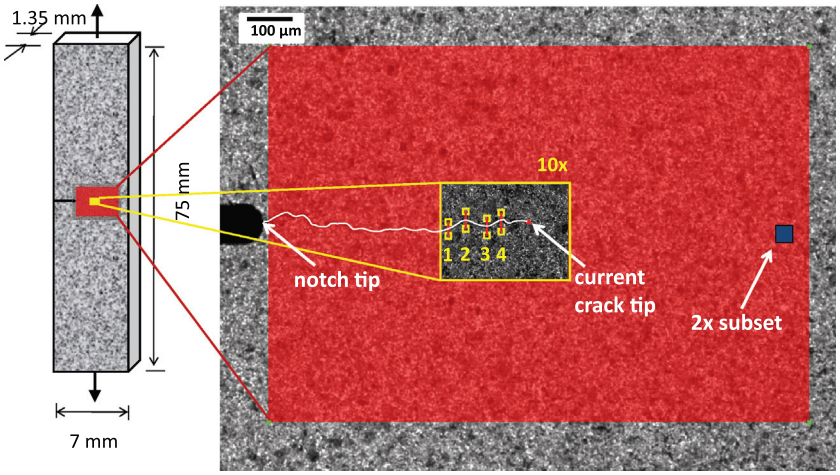

Fig. 4. Schematic of a speckled specimen. The dimensioned specimen is on the left showing the machined notch. The red areas both on the specimen and to the right display the region of interest for the 2× images while the yellow areas display the region of interest for the 10× images. (For interpretation of the references to color in this figure legend, the reader is referred to the web version of this article.)

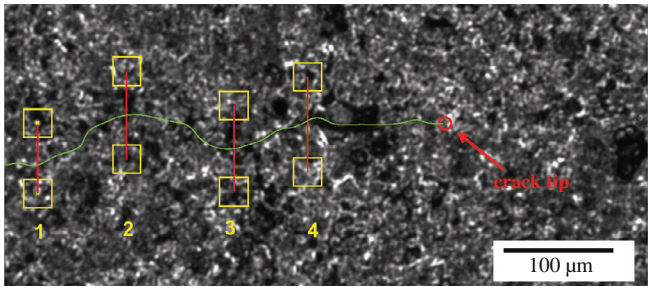

Fig. 5. Digital extensometers placed at various locations along a crack line. The crack tip is circled in red and the crack is outlined in green. The extensometers are comprised of pairs of yellow-boxed subsets. (For interpretation of the references to color in this figure legend, the reader is referred to the web version of this article.)

The macroscale measurement cycles (2×) were analyzed using a full-field DIC method with subset sizes of 41 × 41 pixels at a spacing of 5 pixels (10 μm) in between subsets. Stress intensity factors were calculated using a linear least squares regression method applied to the experimentally measured displacement field. Stress intensity factor was then considered as a function of load in order to calculate the full-field crack closure level using the "full-field effective K" method, as first demonstrated by Carroll et al. [10], where the ratio between the stress intensity factor at opening of the crack and the maximum theoretical stress intensity factor offers the quantified crack closure level. For the purpose of this investigation, unless otherwise stated, the terms 'opening' and 'closing' will be used interchangeably.

3. Results and discussion

3.1. Isothermal fatigue crack closure

Full-field crack closure levels for isothermal fatigue were calculated from macroscale images. Isothermal experiments were either performed in isolation or considered as the first part of the thermal jump experiments. The closure data at the initial T_1 for all thermal jump experiments is shown in Fig. 6 by the blue[2], circle data points in each plot (a–d). Fig. 6(a) demonstrates the isothermal case at RT and displays the specimen's K_I as a function of load. Upon initial loading, the far field stress intensity factor experienced by the specimen increased very little as the crack opened. At a point corresponding to the complete opening of the crack, marked in the figure by a vertical arrow, the stress intensity factor as a function of load becomes parallel to the theoretical K curve. For the room temperature data shown in Fig. 6(a), a closure level ($\frac{K_{open}}{K_{max}}$) of 0.27 was calculated, therefore the specimen experienced 27% less of the peak load than predicted by the theoretical K_I equation. In another RT experiment (not shown), a crack closure level of 0.34 was measured. Thus, over several identical RT experiments a variability of about 0.10 was seen in closure levels measured between specimens. This variability is most likely caused by differences from one sample to another in the form of crack face surface roughness, crack front curvature, local microstructure, etc., all of which affect the levels of crack closure measured.

Fig. 6(b) shows data at isothermal conditions of 300 °C where closure is again seen for the blue data points – note the curvature of the measured stress intensity factor at low loads. The calculated closure level was measured at 0.19. A similar variability in crack closure levels between samples, as was measured in the RT experiments, was also seen for isothermal, 300 °C experiments, shown by Fig. 6(c) and (d) where the measured closure values were 0.39 and 0.28, respectively all at 300 °C. Generally, it was observed that crack closure levels for isothermal experiments were found to be $\frac{K_{open}}{K_{max}} = 0.30 \pm 0.10$. Taking this into consideration, the closure levels measured at 300 °C agreed with those found at RT. Also fitting within this range of variability was an isothermal experiment performed at 550 °C (not shown) which resulted in a crack closure level of 0.27. For the temperature range explored here, closure levels were not significantly affected by temperature under isothermal conditions. The microscale DIC results provide more insight into crack closure by furnishing the variation of *local* opening/closing.

When analyzing images taken at 10× magnification (0.4 μm/pixel), digital extensometers were placed behind the crack tip, on either side of the crack line, as shown in Fig. 5 [33,11,10]. The amount of crack closure measured is affected by the location of the digital extensometers along the crack line [7]. Each gauge tracks the opening and closing of the crack at its specific position along the crack line, as a function of load amplitude and distance from the crack tip, and each extensometer therefore outputs a different, *local* closure level. Note, that in most cases, the opening and closure loads are similar, but not exactly the same. We will not be distinguishing between the two unless specifically stated otherwise.

Fig. 7 shows the load–displacement results of the isothermal RT experiment, where seven extensometers (only three are shown here) were placed along the crack length, from 302 μm to 102 μm behind the crack tip. The local opening and closing load levels increase as the crack tip is approached, as expected [10], demonstrating that more crack closure is occurring closer to the crack tip. Furthest from the crack tip (Fig. 7(a)) the calculated closure level was 0.40 (at 302 μm from the crack tip) while closest to the crack tip (Fig. 7(c)) the closure level was 0.64 (at 102 μm from the crack tip). The point closest to the crack tip is most shielded by the compressive forces along the flanks of the crack due to the presence of closure and therefore a greater force is required to fully open the crack at that point.

Fig. 8 shows the extensometer placement and the measured results for an experiment at 300 °C. The same unzipping phenomenon is again observed at high temperature as at RT. In this 300 °C experiment, there is evidence of serrated loading in the load vs. displacement curves that increase as the gauges approach the crack tip. This is most likely a result of the Portevin-Le Catelier effect (PLC) which is known to exist at this alloy at elevated temperatures [27,39].

Fig. 9 displays a combined plot of the microscale closure data both at RT and 300 °C. As was demonstrated in the gauge displacement as a function of load, closure levels are largest, closest to the crack tip. Local opening levels are shown by circles while local closing levels are shown by triangles.

As is shown in Fig. 1, there is a 35 GPa reduction of elastic modulus as well as a 130 MPa reduction of yield strength of Hastelloy X over the temperature range investigated here. Plasticity, being a prominent driving force for crack closure, is affected by temperature. Though our isothermal results indicated that isothermal conditions do not affect the measured crack closure levels, temperature changes within a single experiment, where uncertainties resulting from sample-to-sample variability (such as crack face surface roughness, crack front curvature, and local microstructure) are minimized, have a significant influence on crack closure, as will be seen.

3.2. Fatigue crack closure following thermal jumps

During fatigue cracking, the area in front of the crack tip is affected by competing mechanisms. Here, the mechanisms observed included crack tip blunting, bifurcation, as well as crack closure.

[2] For interpretation of color in Figs. 6 and 11, the reader is referred to the web version of this article.

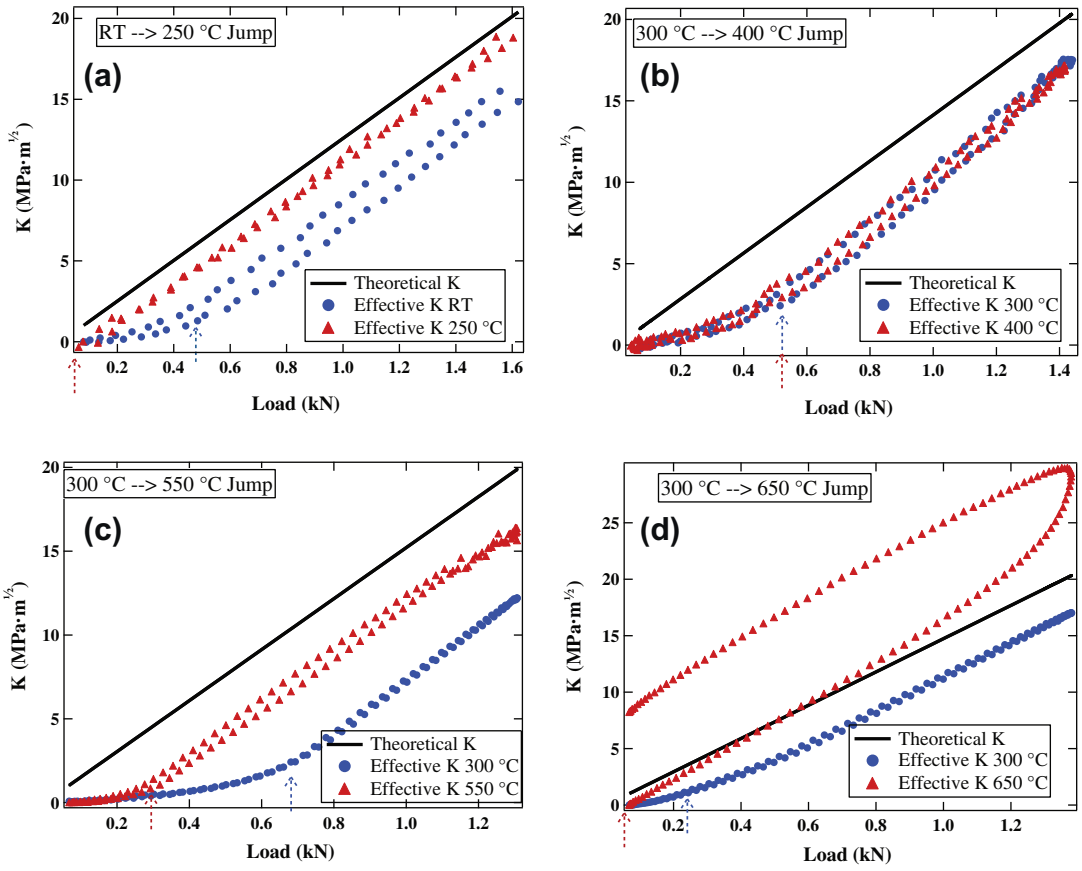

Fig. 6. Comparison of theoretical stress intensity factors and those determined using the KT regression on experimental data curves (a) RT to 250 °C jump, (b) 300–400 °C jump, (c) 300–550 °C jump, and (d) 300–650 °C jump.

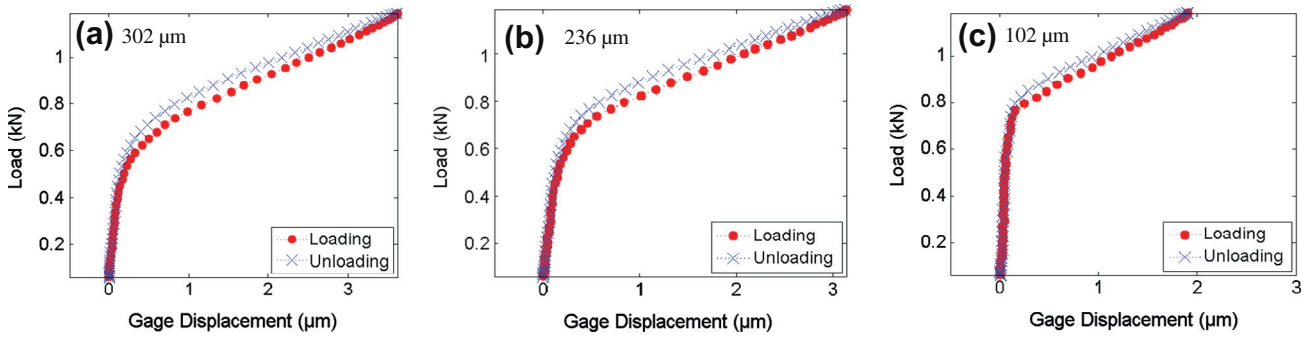

Fig. 7. Load vs. Gauge Displacement curves for the displacement gauges located, from left to right, at (a) 302 μm, (b) 236 μm, and (c) 102 μm from the crack tip for a room temperature experiment.

The Wheeler model has been studied by numerous researchers, and states that following a mechanical, tensile overload, the crack tip region experiences compressive residual stresses in an area proportional to the plastic zone size, which cause a retardation of fatigue crack propagation [14,15,40,41,18,19,21,42]. This model predicts the crack propagation to no longer be reduced when the crack has grown through the plastic zone caused by the tensile overload. Crack tip blunting is also seen following tensile overloads [16,15,19] and is viewed as a prominent mechanism in the retardation of the fatigue crack's growth. Elber [3,4] connected this to the crack closure phenomenon, stating that plasticity-induced crack closure could also be responsible for the transient retardation phenomenon due to overloads, where the elastic region of material surrounding the enlarged plastic zone ahead of the crack tip causes residual compressive stresses thereby reducing crack propagation rates within this plastic zone. Suresh [17], postulated that crack closure could not be the dominant mechanism involved in retarding the crack growth rate following an overload. Crack bifurcation has also been cited as a mechanism responsible for slower crack growth rates [43,44].

Consider a thermal jump experiment from RT to 250 °C, the macroscopic results of which are shown in Fig. 6(a) where the RT data is the last measurement cycle at RT (before the overload occurs) shown by blue, circular data points and the 250 °C data is the third measurement cycle of the thermal overload at 250 °C, shown by red, triangular data points. The room temperature crack closure level was measured to be 0.27 and the point of crack tip opening is shown by a vertical arrow. Following the temperature

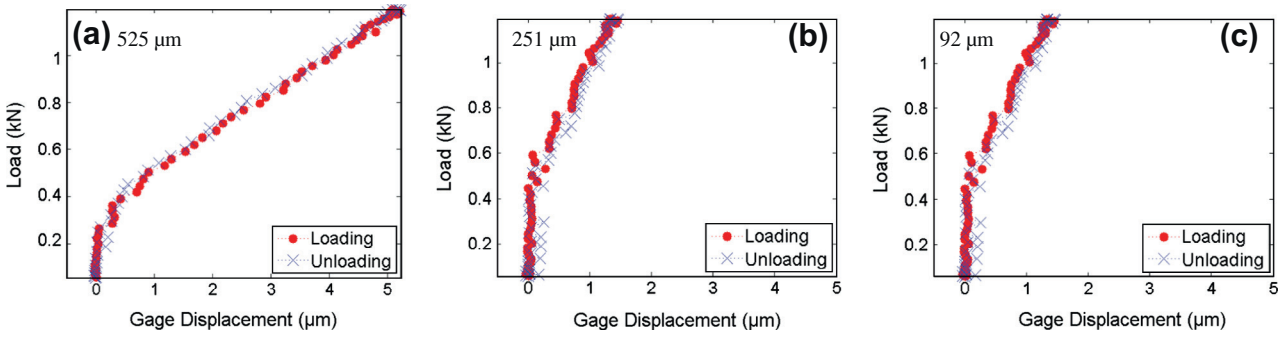

Fig. 8. Load vs. Gauge Displacement curves for the displacement gages located, at (a) 525 μm, (b) 251 μm, and (c) 92 μm from the crack tip for a 300 °C experiment. Serrated loading is present due to the PLC effect.

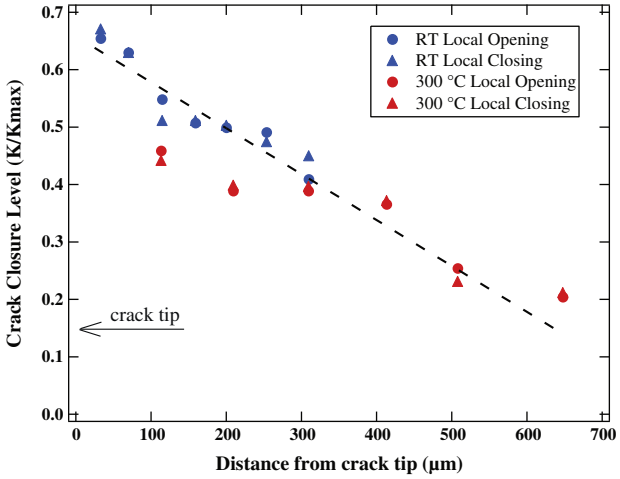

Fig. 9. Local crack closure and crack opening as a function of distance from the crack tip at room temperature and 300 °C. The data points corresponding with opening levels are shown as circles while the data points corresponding with closing levels are shown as triangles.

jump from RT to 250 °C, the specimen no longer experienced any crack closure, (the experimental stress intensity factor as a function of load for the third cycle at T_2 is linear, and agrees very closely with the theoretical curve in Fig. 6(a)). The very slight offset between the two curves is most likely due to the theoretical curve beginning at the origin while the loading cycle for the specimen started slightly above zero load (since $R > 0$).

In a different thermal jump experiment, at T_1 of 300 °C, the specimen experienced a pre-jump crack closure level of 0.19. This is shown by Fig. 6(b). After the jump in temperature of 100 °C to T_2 of 400 °C, the closure level decreased slightly to 0.18. These two crack closure levels are essentially the same within the resolution limits of the measurement techniques. This suggests that a temperature jump from 300 °C to 400 °C is not sufficient to affect the level of crack closure measured. From the material property values shown in Fig. 1, one can see that the elastic modulus reduces by 5 GPa while the yield stress reduces by 20 MPa when the temperature jumps from 300 °C to 400 °C (compared to 10 GPa and 60 MPa due to the jump from RT to 250 °C).

Fig. 6(c) shows K_I as a function of load before and after a thermal jump from 300 °C to 550 °C. The specimen experienced a pre-jump crack closure level of 0.39 at the T_1 of 300 °C. When the temperature jumped to the T_2 of 550 °C, the closure level reduced to 0.15. The temperature change from 300 °C to 550 °C is accompanied by a reduction in the elastic modulus of the material of 15 GPa and in the yield stress of 50 MPa. The temperature difference of 250 °C was similar to the RT to 250 °C jump. However, in the RT to 250 °C thermal jump, no crack closure was measured following the temperature jump. Consequently, only considering the change in temperature between T_1 and T_2 is not an adequate metric in predicting the amount of crack closure that will result. Considering the material properties between the RT to 250 °C and the 300–550 °C jump, the latter experienced a 50 MPa reduction in yield stress with the temperature jump while the former experienced a 60 MPa reduction. Conversely, the 300–550 °C jump experiences a more pronounced decrease in the elastic modulus compared to the RT to 250 °C jump (15 GPa vs. 10 GPa). These material parameters, along with the change in temperature, the change in the plastic zone in front of the crack tip, the bifurcation of the crack, and the crack opening displacement, likely influence the crack closure behavior.

Considering a final thermal jump, from 300 °C to 650 °C, a T_1 of 300 °C resulted in a pre-jump closure level of 0.28 as shown in Fig. 6(d). T_2 was chosen as 650 °C in order to create a temperature change greater than 300 °C while keeping the change in yield stress between T_1 and T_2 constant compared to the 300–550 °C jump (since the yield stress is the same at 550 °C and 650 °C). The elastic modulus between 300 °C and 650 °C decreases by 20 GPa while the yield stress decreases by 50 MPa. The change in yield stress is therefore the same for both the 300–550 °C and 300 °C and 650 °C jumps. However, in contrast to the 300–550 °C thermal jump, the 300–650 °C thermal jump experiment exhibited a complete elimination of crack closure, similar to the room temperature to 250 °C thermal jump. Considering solely the change in yield stress of the material between T_1 and T_2 is therefore also not an adequate metric for predicting the resulting crack closure levels. Comparing RT to 250 °C and the 300 °C and 650 °C thermal jump (which both experienced an elimination of crack closure), the elastic modulus decreases by 10 GPa and 20 GPa respectively, and the yield stress decreases by 60 MPa and by 50 MPa, respectively. The 300 °C and 650 °C thermal jump therefore, experiences a smaller decrease in the yield stress but a larger decrease in the elastic modulus compared to the RT to 250 °C jump, even though, following the thermal jump, neither experiment experienced crack closure.

A figure summarizing these isothermal and thermal jump results can be seen in Fig. 10, showing the crack closure level plotted as a function of temperature. The isothermal experiments are denoted as diamond data points with vertical scatter bars showing the range of closure levels calculated under each isothermal condition (except for the 550 °C isothermal condition where only a single, isothermal experiment was completed). Triangular data points are shown for the thermal jump experiments with an arrow connecting the initial T_1 temperature to its T_2 counterpoint.

In these thermal jump experiments, an increase in temperature causes a change in plastic zone size, similar to a mechanical

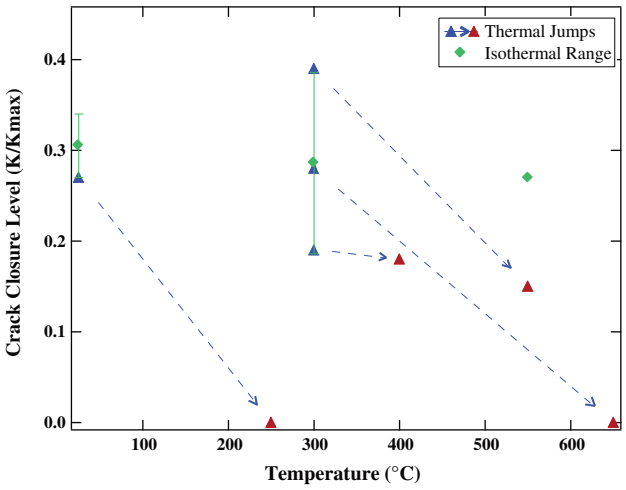

Fig. 10. Crack closure data for both isothermal and thermal jump experiments. Crack closure is plotted as a function of temperature. The isothermal experiments are denoted as diamond data points with vertical scatter bars showing the range of closure levels calculated under each isothermal condition while the thermal jump experiments are denoted as triangular data points shown with an arrow connecting the initial T_1 temperature to its T_2 counterpoint.

overload. Using the Von Mises elastic estimate for the radius of the plane-stress plastic zone,

$$r_{pl-\sigma} = \frac{1}{4\pi}\left(\frac{K_I}{\sigma_y}\right)^2 (1 + \cos\theta + 1.5(\sin\theta)^2), \quad (4)$$

the plastic zone was plotted as a function of position [32], and overlaid onto the vertical displacement contours in Fig. 11. In Fig. 11(a), the solid black line shows the plastic zone estimate at the peak load of the last measurement cycle at RT before the thermal jump while Fig. 11(b) shows the plastic zone estimate at the peak load of the third measurement cycle at the thermal jump of 250 °C. The solid blue contour lines and the dashed red contour lines show a comparison between the experimentally measured DIC, vertical displacement field component and the fitted KT-dominant field, respectively [10]. As is to be expected, similar to the case of a mechanical overload, the plastic zone size resulting from the thermal jump from RT to 250 °C (shown in Fig. 11(b)) is considerably larger than the plastic zone size resulting from the fatigue cracking at RT (Fig. 11(a)). Note that these calculated plastic zone shapes and sizes are merely representative. Actual plastic zones can be measured by using DIC. Fig. 12 shows the strain field in the vertical direction at peak load for both RT (Fig. 12(a)) and 250 °C (Fig. 12(b)). These experimental images correspond to the point of maximum loading and are also used in Fig. 11(a) and (b). The measurement cycles at the T_1 temperature were performed just before overload to the T_2 temperature (and therefore, at the same crack length). The crack line is found behind the horizontal region of higher strain (shown in red on the color bar on the right) with a white dot showing where the crack tip is. The plastic zone extends as two lobe-like shapes from the end of the crack tip. In Fig. 12(a) and (b), the experimental plastic zones can be inferred from the experimental vertical strain fields as the regions of strain exceeding 0.3%. The experimental plastic zone is larger at the more elevated temperature as demonstrated by the comparison between the strain levels in Fig. 12(b) and in Fig. 12(a). It is also important to note that, since the reference or undeformed state for the analysis done in Fig.12 was chosen as the initial, zero load image of the same cycle as the maximum load point shown, Fig. 12 shows the contour plots of the *incremental* vertical strain at maximum load.

The radius of the Von Mises calculated plastic zone directly ahead of the crack tip can be estimated for 300 °C to be roughly 0.57 mm. The corresponding value at 550 °C is 0.85 mm. This results in a change in plastic zone size of 0.25 mm due to the temperature jump from 300 °C to 550 °C. Similarly, there is a theoretical change in plastic zone of 0.14 mm due to the RT to 250 °C thermal jump. As discussed previously, the RT to 250 °C thermal jump resulted in the elimination of crack closure following the thermal jump while the 300–550 °C jump resulted in the reduction (not elimination) of closure, even with a larger change in the size of the plastic zone. A more significant change in the size of the plastic zone ahead of the crack tip therefore does not directly determine whether or not closure will be eliminated following an overload. Thus, the change in the plastic zone size alone is also not an adequate metric in predicting the amount of crack closure that will result from a thermal jump. To understand why the elimination of crack closure seen here occurs immediately following the thermal jump requires investigation not only of the enlargement of the plastic zone, but also the nature of the opening directly behind the crack tip.

An optical microscope image of the crack tip region, taken at 50× magnification after the completion of the RT to 250 °C experiment, is shown in Fig. 13(a). The black spots are most likely pitting which occurred during polishing of the sample. (Note that in Fig. 13(a–c), the DIC speckle pattern has been removed in order to better view the crack tip.) Blunting of the crack tip, crack bifurcation, and significant crack opening are evident. The increased plasticity at the higher temperature causes blunting, which increases the near-tip crack opening displacement resulting in reduced crack closure. Though the mechanical overload data found in the literature also shows evidence of blunting [16,15,19], the thermal jump case is more complex. During the heating of a specimen, the entire specimen is affected by the increase in temperature and therefore, the entire specimen undergoes changes in its material parameters such as elastic modulus and yield stress.

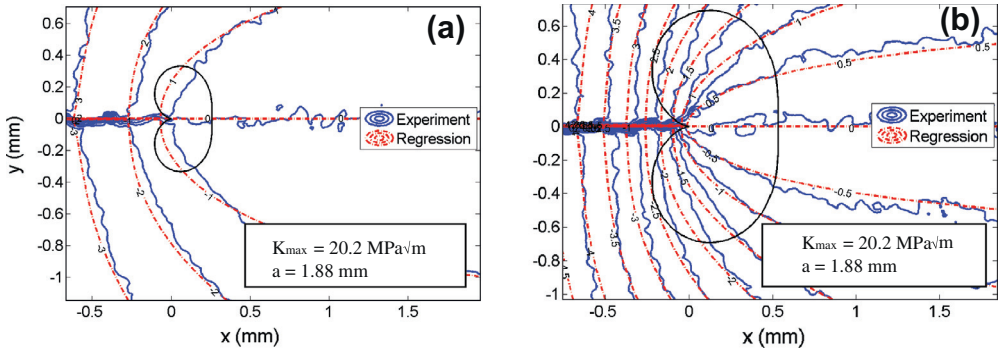

Fig. 11. (a) Vertical displacement contours at maximum load at RT, just prior to the thermal jump. (b) Vertical displacement contours at maximum load at the thermal jump to 250 °C. In each image, the theoretical plane-stress plastic zone is outlined in black.

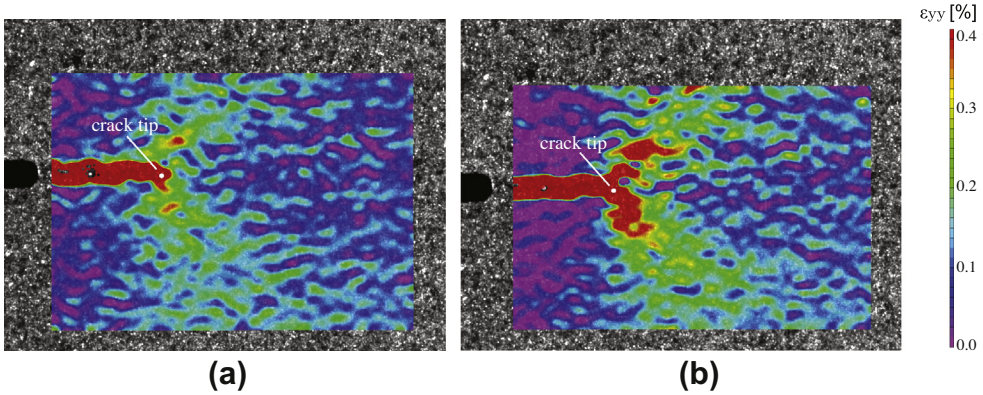

Fig. 12. (a) Vertical strain field at maximum load at RT. (b) Vertical strain field at maximum load following a thermal jump to 250 °C. The crack tip is shown by a white dot.

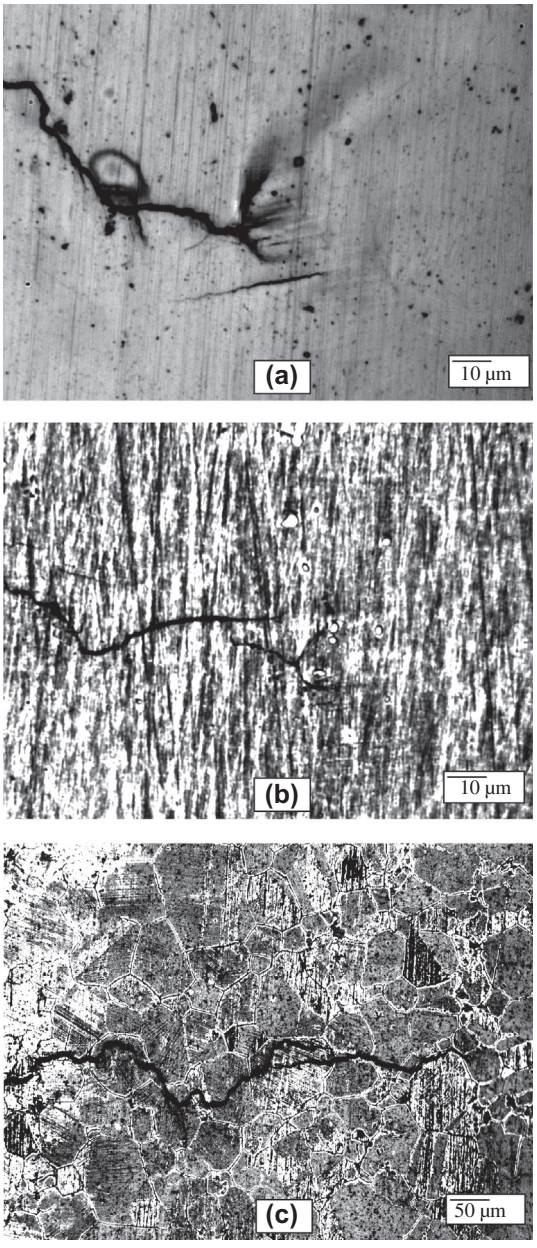

Fig. 13. Post-mortem image of crack tips at (a) 50× magnification for RT to 250 °C jump, (b) 50× magnification for 300–550 °C jump, and (c) 10× magnification for 300–650 °C jump.

During a mechanical overload, it is the region just in front of the crack tip that experiences the greatest changes. In the case of a heating, the stress state of the entire material, including the region of residual compressive stresses, relaxes. This results in a complete opening of the crack and blunting of the crack tip. The crack tip, no longer considered "sharp" after the first measurement cycle at T_2, would now need to reinitiate before closure could reemerge. The enlarged plastic zone should affect the crack growth rate ahead of this overload position as well as the evolution of closure and crack propagation rate as the crack tip continues to grow through the enlarged plastic zone. Fig. 13(b) shows a post-mortem image taken at 50× magnification after the completion of the 300–550 °C thermal jump experiment. Crack bifurcation as well as crack opening is visible. Fig. 13(c) displays a 10× magnification post-mortem image of the 300–650 °C experiment. At the lower magnification more of the crack path is visible. Grains have been exposed in this image due to exposure to the T_2 of 650 °C. The crack path crosses grains as well as skirting along grain boundaries and crack bifurcation is evident.

3.3. Fatigue crack closure following thermal overloads

In analogy to a mechanical overload experiment, thermal overload experiments were performed in this work. The crack was grown at a T_1 of 300 °C to a total crack length of 2.00 mm, a three cycle thermal overload at a T_2 temperature of 650 °C was performed at this same crack length, and finally, crack growth was continued at the original T_1. Crack closure, characterized by full-field DIC measurements, was quantified at various crack lengths while growing the fatigue crack post-overload by performing measurement cycles periodically as the crack advanced. Prior to the overload, crack closure was quantified at a crack length of 2.00 mm at T_1 as 0.16. After the overload to 650 °C, the crack closure was found to be eliminated. In Fig. 14 the crack closure level throughout the overload experiment, both pre- and post-overload, is summarized. The vertical, dashed line illustrates the crack length where the thermal overload occurred. Fig. 14 shows, although crack closure was eliminated immediately following the thermal overload, crack closure levels subsequently increased once the thermal conditions were reestablished at T_1 and fatigue loading was continued to advance the crack beyond the overload plastic zone. The figure also displays two experimental images, one at maximum loading in the 300 °C measurement cycle just prior to the overload and the other at maximum loading of the first 300 °C measurement cycle just post-overload, both at the same crack length. Opening of the crack tip is very visible in the post-overload image.

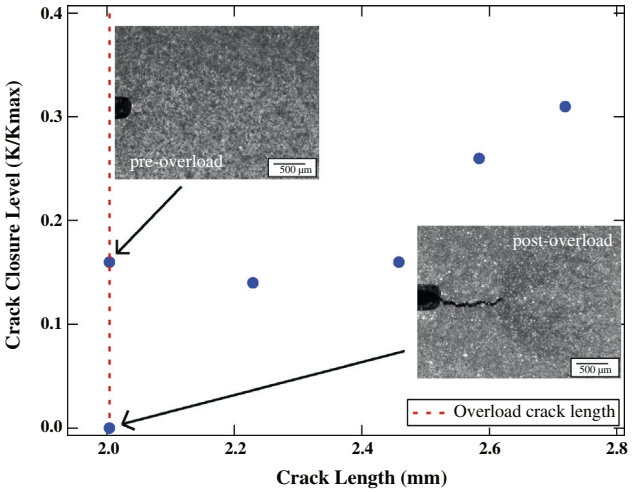

Fig. 14. Fatigue crack closure level as a function of crack length for a 300–650 °C thermal overload.

As the crack grew after the overload, crack closure levels rose from 0.0 to 0.14, 0.16, 0.26, and 0.31 at crack lengths of 2.23, 2.46, 2.58, and 2.72 mm, respectively. The crack remained at a crack length of a = 2.72 mm for another 100,000 cycles before the experiment was halted. Fatigue crack growth rates have been shown to return to nominal, pre-overload levels when grown outside of the affected plastic zone caused by a tensile overload in both experimental and finite element studies [15]20. Here, crack closure levels post-overload increased past the levels which were seen prior to the overload.

Fig. 15 shows the crack length, a, as a function of the number of cycles, N for the thermal overload experiment. The dashed red line represents the crack length, a = 2.00 mm, where the thermal overload occurred and the dashed green line represents the crack length, a = 2.90 mm, where the crack should have (based on a calculated estimate from Eq. (4)) grown out of the enlarged plastic zone created by the thermal overload to 650 °C. Fig. 15 shows a slight retardation in crack growth rate until a little before the estimated boundary of the elasto-plastic zone. As stated earlier, the crack ceased propagating after this point in crack growth. As the crack tip propagated through the thermal overload plastic zone,

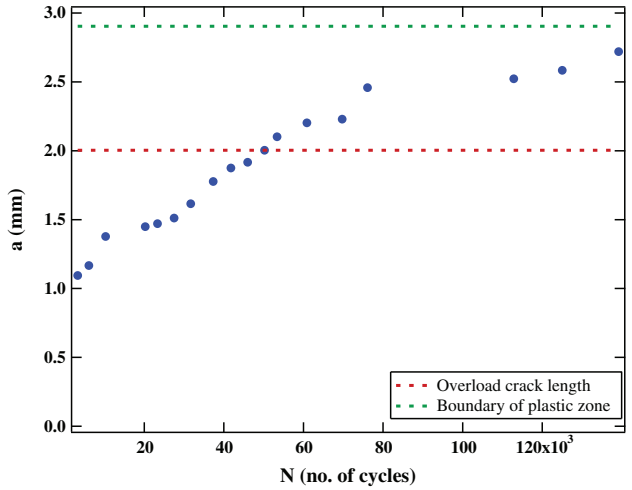

Fig. 15. a vs. N for the thermal overload at 300 °C. The red dashed line signifies where the thermal overload to 650 °C occurred and the green dashed line signifies where the crack should have grown out of the plastic zone created by the thermal overload. (For interpretation of the references to color in this figure legend, the reader is referred to the web version of this article.)

the compressive forces on the crack flanks would be expected to increase, thereby slowing the crack advance. In this case, it appears that the crack closure forces experienced by the crack as it grew through the thermal overload's plastic zone were sufficient enough to cease crack propagation before the crack closure levels could return to nominal, pre-overload levels.

4. Conclusions

This investigation provided a multiscale examination of the effects of temperature on fatigue crack closure of Hastelloy X. Hastelloy X was chosen for the investigation due to its high temperature, deformation resistance. In order to obtain a complete understanding of the effects that temperature has on fatigue crack closure, three different experiments were performed: (i) isothermal experiments at RT, 300 °C, and 550 °C, (ii) thermal jump experiments with temperature jumps from RT to 250 °C, 300 °C to 400 °C, 300 °C to 550 °C, and 300 °C to 650 °C, and (iii) a thermal overload experiment from 300 °C to 650 °C.

Two different length scales were considered, each using a different digital image correlation analysis methodology. Macroscale DIC measurements at 2× magnification (2 μm/pix) provided full-field crack closure measurements. *Local* crack closure measurements, as a function of distance behind the crack tip, were obtained using microscale DIC measurements at 10× magnification (0.4 μm/pix).

The macroscale, isothermal experiments, conducted at RT, 300 °C, and 550 °C, did not show a significant crack closure dependence on temperature. Sample-to-sample variability resulted in crack closure levels of 0.30 ± 0.10. The microscale, isothermal experiments showed similar results. As expected, local crack closure levels increased as the crack tip was approached.

Through a series of thermal jump experiments it was determined that temperature jumps within a single experiment, where sample to sample variability no longer exists, do affect crack closure levels. However, only considering the change in temperature between T_1 and T_2 was not an adequate metric in predicting the change in crack closure levels that resulted following the temperature elevation. Individually considering the change in yield stress or plastic zone size were also demonstrated to be inadequate metrics for predicting the amount of crack closure that will result from a thermal jump. Consequently, the interplay between these mechanisms was determined to be complex and temperature dependent.

Of direct significance were crack tip blunting and bifurcation observed in post-mortem imaging of specimens. This blunted crack would need to reinitiate a sharp crack before crack closure could reemerge and would be advantageous towards delaying continued fatigue crack growth until the crack tip was able to reinitiate. Delayed crack growth following an overload was supported by the a vs. N curve. This curve showed crack growth rate retardation following the overload. Eventually, crack closure levels increased such that crack growth ceased. While the change in yield stress, elastic modulus, plastic zone size, and temperature caused by the jump in thermal conditions all contributed, the resultant crack tip opening behavior was shown to play the dominant role in reducing or eliminating fatigue crack closure.

In summary, thermal effects on crack growth and crack closure behavior are still not well understood. To our knowledge, no studies have specifically examined thermal jump and thermal overload experiments such as those shown here. There are a number of interacting variables that affect crack closure levels in thermal environments, and further study will be necessary to fully understand these interactions. This work provides experimental observations of these interactions and sheds light on the expected behavior of fatigue cracks in thermally active environments.

Acknowledgements

This work is based on research sponsored by Air Force Research Laboratory through agreement No. FA8650-06-2-3620 under the auspices of the Midwest Structural Sciences Center and by NASA under award No. NNX11AJ95H. The U.S. Government is authorized to reproduce and distribute reprints for Governmental purposes notwithstanding any copyright notation thereon.

References

[1] Paris P, Erdogan F. A critical analysis of crack propagation laws. J Basic Eng 1963;85(4):528. http://dx.doi.org/10.1115/1.3656900.
[2] McEvily Jr A, Boettner R. On fatigue crack propagation in FCC metals. Acta Metall 1963;11:725–43.
[3] Elber W. Fatigue crack closure under cyclic tension. Eng Fract Mech 1970;2:37–45.
[4] Elber W. The significance of fatigue crack closure. Damage tolerance in aircraft structures ASTM STP 4. American Society for Testing and Materials; 1971. p. 230–42.
[5] Suresh S, Ritchie R. Near-threshold fatigue crack propagation: a perspective on the role of crack closure. The Metallurgical Society of AIME; 1984.
[6] Sehitoglu H. Crack opening and closure in fatigue. Eng Fract Mech 1985;21(2):329–39.
[7] Davidson D. Fatigue crack closure. Eng Fract Mech 1991;38(6):393–402. http://dx.doi.org/10.1016/0013-7944(91)90091-E.
[8] Horng J, Fine M. Near-threshold fatigue crack propagation rates of dual-phase steels. Mater Sci Eng 1984;67(2):185–95. http://dx.doi.org/10.1016/0025-5416(84)90050-8.
[9] Vecchio R, Crompton J, Hertzberg R. The influence of specimen geometry on near threshold fatigue crack growth. Fatigue Fract Eng Mater Struct 1987;10(4):333–42.
[10] Carroll J, Efstathiou C, Lambros J, Sehitoglu H, Hauber B, Spottswood S, Chona R. Investigation of fatigue crack closure using multiscale image correlation experiments. Eng Fract Mech 2009;76(15):2384–98. http://dx.doi.org/10.1016/j.engfracmech.2009.08.002.
[11] Riddell W, Piascik R, Sutton M, Zhao W, McNeill S, Helm J. Determining fatigue crack opening loads from near-crack-tip displacement measurements, ASTM STP 1343; 1999.
[12] Sutton MA, Zhao W, McNeill SR, Helm JD, Piascik RS, Riddell WT. Local crack closure measurements: development of a measurement system using computer vision and a far-field microscope, vol. 2. ASTM STP 1343; 1999.
[13] Willenborg J, Engle R, Wood H. A crack growth retardation model using an effective stress concept. Tech rep, Air force flight dynamics laboratory, director of laboratories, air force systems command, wright patterson air force base ohio; 1971.
[14] Wheeler O. Spectrum loading and crack growth. J Basic Eng 1972;94:181–6.
[15] Matsuoka S, Tanaka K, Kawahara M. The retardation phenomenon of fatigue crack growth in HT80 steel. Eng Fract Mech 1976;8(3):507–23. http://dx.doi.org/10.1016/0013-7944(76)90005-9.
[16] Brown R, Weertman J. Effects of tensile overloads on crack closure and propagation rates in 7050 aluminum. Eng Fract Mech 1978;10:867–78.
[17] Suresh S. Micromechanisms of fatigue crack growth retardation following overloads. Eng Fract Mech 1983;18(3):577–93. http://dx.doi.org/10.1016/0013-7944(83)90051-6.
[18] Lu Y, Li K. A new model for fatigue crack growth after a single overload. Eng Fract Mech 1993;46(5):849–56.
[19] Halliday MD, Zhang JZ, Poole P, Bowen P. In situ SEM effects of an overload on small fatigue crack growth at two different load ratios in 2024-T351 aluminium alloy. Science 1997;19(4):273–82.
[20] Roychowdhury S, Dodds Jr RH. Effects of an overload event on crack closure in 3-d small-scale yielding: finite element studies. Fatigue Fract Eng Mater Struct 2005;28:891–907.
[21] Borrego L, Ferreira J, Pinho da Cruz J, Costa J. Evaluation of overload effects on fatigue crack growth and closure. Eng Fract Mech 2003;70(11):1379–97. http://dx.doi.org/10.1016/S0013-7944(02)00119-4.
[22] Suresh S. Fatigue of materials. Cambridge University Press; 1998.
[23] Babu MN, Dutt BS, Venugopal S, Sasikala G, Bhaduri AK, Jayakumar T, Raj B. On the anomalous temperature dependency of fatigue crack growth of SS 316(N) weld. Mater Sci Eng A 2010;527(20):5122–9. http://dx.doi.org/10.1016/j.msea.2010.04.075.
[24] Kokini K. On the use of the finite element method for the solution of a cracked strip under thermal shock. Eng Fract Mech 1980;24(6):843–50.
[25] Giannopoulos G, Anifantis N. Finite element analysis of crack closure in two-dimensional bodies subjected to heating. Comput Struct 2005;83(4–5):303–14. http://dx.doi.org/10.1016/j.compstruc.2004.10.008.
[26] Abuzaid WZ, Sangid MD, Carroll JD, Sehitoglu H, Lambros J. Slip transfer and plastic strain accumulation across grain boundaries in Hastelloy X. J Mech Phys Solids 2012;60(6):1201–20. http://dx.doi.org/10.1016/j.jmps.2012.02.001.
[27] Swaminathan B, Lambros J, Sehitoglu H. Investigation of the portevin-le chatelier effect at elevated temperatures in Hastelloy X using digital image correlation. Int J Plast; submitted for publication.
[28] Jonnalagadda K, Chasiotis I, Yagnamurthy S, Lambros J, Pulskamp J, Polcawich R, Dubey M. Experimental investigation of strain rate dependence of nanocrystalline pt films. Exp Mech 2010;50:25–35.
[29] Padilla H, Lambros J, Beaudoin A, Robertson I. Relating inhomogeneous deformation to local texture in zirconium through grain-scale digital image correlation strain mapping experiments. Int J Solids Struct 2012;49(1):18–31. http://dx.doi.org/10.1016/j.ijsolstr.2011.09.001.
[30] Efstathiou C, Sehitoglu H, Carroll J, Lambros J, Maier H. Full-field strain evolution during intermartensitic transformations in single-crystal NiFeGa. Acta Mater 2008;56(15):3791–9. http://dx.doi.org/10.1016/j.actamat.2008.04.033.
[31] Haynes international high-temperatue alloys: Hastelloy X alloy <http://www.haynesintl.com/pdf/h3009.pdf>.
[32] Dowling NE. Mechanical behavior of materials: engineering methods for deformation, fracture, and fatigue. Prentice-Hall Inc; 1999.
[33] Sutton M, Wolters W, Peters W, Ranson W, McNeill S. Determination of displacements using an improved digital correlation method. Image Vis Comput 1983;1(3):133–9.
[34] Sutton MA, Orteu J-J, Schreier HW. Image correlation for shape, motion and deformation measurements. Springer; 2009.
[35] Lyons J, Liu J, Sutton M. High-temperature deformation measurements using digital-image correlation. Exp Mech 1996;36(March):64–70.
[36] Grant B, Stone H, Withers P, Preuss M. High-temperature strain field measurement using digital image correlation. J Strain Anal Eng Des 2009;44(4):263–71. http://dx.doi.org/10.1243/03093247JSA478.
[37] Pan B, Wu D, Wang Z, Xia Y. High-temperature digital image correlation method for full-field deformation measurement at 1200 °C. Measure Sci Technol 2011;22(1):015701. http://dx.doi.org/10.1088/0957-0233/22/1/015701.
[38] Pataky GJ, Sehitoglu H, Maier HJ. High temperature fatigue crack growth of Haynes 230. Mater Character 2012;75:1–10. http://dx.doi.org/10.1016/j.matchar.2012.09.012.
[39] Castelli MG, Miner RV, Robinson DN. Thermomechanical fatigue behavior of materials: thermomechanical deformation behavior of a dynamic strain aging alloy, Hastelloy X. American Society for Testing and Materials STP 1186, 1993.
[40] Gan D, Weertman J. Crack closure and crack propagation rates in 7050 aluminum. Eng Fract Mech 1981;15(1–2):87–106. http://dx.doi.org/10.1016/0013-7944(81)90108-9.
[41] Bray G, Reynolds A, Starke Jr EA. Mechanisms of fatigue crack retardation following single tensile overloads in powder metallurgy aluminum alloys. Metall Trans A 1992;23:3055–66.
[42] Pereira M, Darwish F, Camarão A, Motta S. On the prediction of fatigue crack retardation using Wheeler and Willenborg models. Mater Res 2007;10(2):101–7. http://dx.doi.org/10.1590/S1516-14392007000200002.
[43] Kotoul M, Sevecek O, Vyslouzil T. Crack growth in ceramic laminates with strong interfaces and large compressive residual stresses. Theor Appl Fract Mech 2012;61:40–50. http://dx.doi.org/10.1016/j.tafmec.2012.08.005.
[44] Jin H, Lu W-Y, Haldar S, Bruck HA. Microscale characterization of granular deformation near a crack tip. J Mater Sci 2011;46(20):6596–602. http://dx.doi.org/10.1007/s10853-011-5608-3.